Measurement of the wave-front aberration of the eye by a fast psychophysical procedure

J. C. He, S. Marcos, R. H. Webb, and S. A. Burns

Schepens Eye Research Institute, 20 Staniford Street, Boston, Massachusetts 02114

We used a fast psychophysical procedure to determine the wave-front aberrations of the human eye *in vivo*. We measured the angular deviation of light rays entering the eye at different pupillary locations by aligning an image of a point source entering the pupil at different locations to the image of a fixation cross entering the pupil at a fixed location. We fitted the data to a Zernike series to reconstruct the wave-front aberrations of the pupil. With this technique the repeatability of the measurement of the individual coefficients was 0.019 μm. The standard deviation of the overall wave-height estimation across the pupil is less than 0.3 μm. Since this technique does not require the administration of pharmacological agents to dilate the pupil, we were able to measure the changes in the aberrations of the eye during accommodation. We found that administration of even a mild dilating agent causes a change in the aberration structure of the eye. © 1998 Optical Society of America [S0740-3232(98)03509-1]

OCIS codes: 330.5510, 330.5370, 010.1080, 330.7310.

1. INTRODUCTION

The optical performance of the human eye is not ideal: it has long been recognized that the eye is diffraction limited only for relatively small pupil diameters.[1–5] For larger-diameter pupils the aberrations of the eye's optics come into play, limiting visual acuity and contrast sensitivity. With the development of new surgical techniques for correcting the optics of the eye there has been a renewed interest in developing accurate, reproducible techniques for measuring the wave-front aberrations of the human eye as well as for studying changes in the optics of the eye with age.[6–8] Overall, the approaches currently being used to measure the monochromatic wave-front aberrations of the pupil can be divided into optical and psychophysical techniques. The optical techniques include analysis of aerial images of the retinal point-spread function,[5,9] objective aberroscope measurements,[10] analysis of the deviation of small pencils of light onto the retina,[11] and the use of Hartmann–Shack wave-front sensors.[12,13] These optical techniques have the advantage that they are fast, reproducible, and reliable. However, they have the potential disadvantage that they require the use of bright lights and the application of mydriatics to yield wave-front aberrations for relatively large pupils. While the psychophysical techniques in current use can be fast,[14] there is a trade-off between accuracy and speed. The most accurate techniques[15,16] tend to be slower. The advantage of the psychophysical techniques is that they can be used at light levels low enough that the natural pupil is large. Thus it is generally thought that these techniques require long session times or trained subjects.[17] Therefore the use of these techniques has generally been restricted to measuring the aberrations of the eye along a single pupillary axis.[15,16]

Here we describe an implementation of a psychophysical technique for measuring the monochromatic wave-front aberrations of the eye based on the spatially re-solved refractometer described by Webb *et al.*[18] The modifications described allow us to measure a complete set of wave-front aberrations in 3–4 min. First we describe the modified design of the instrument. We then discuss the accuracy of the fitting procedure with the help of computer simulations as well as the performance of the device when known refractive errors are introduced and an artificial eye is used. Next we characterize the reproducibility of the spatially resolved refractometer for measurements *in vivo*, examining changes in wave-front aberrations both within and across days. Finally, as an example of the potential utility of the technique, we examine changes in the wave-front aberrations of the eye with the application of mydriatics and changes in the accommodative stimulus.

2. METHODS

A. Apparatus

The principle of the spatially resolved refractometer has been described in detail elsewhere.[18] Briefly stated, if the eye were diffraction limited and focused at infinity, then light originating from a distant point source that entered the pupil at different locations would be brought to a focus at a single retinal location. In actuality aberrations of the eye's optics cause light entering from different pupillary locations to be directed to different retinal locations; that is, the image of the point source is blurred. The angular deviation of the light at each point in the pupil is a measure of the aberration at that point.[15,16,18–21] We measure the angular deviation by determining the change in angle necessary to bring the retinal image of the point source back to a standard location, in our case, to the center of a fixation cross.

The original implementation of the spatially resolved refractometer was not well suited for testing naïve subjects. Thus we redesigned the instrument, adding pupil

monitoring, more rapid and reproducible pupil positioning, the ability to control for the refractive state of the eye without changing the magnification of the pupil, and the ability to vary the pupil diameter of the fixation channel. To do this we built a three-channel Maxwellian view system (Fig. 1). Separate channels are used for providing the test stimulus, a reference stimulus with adjustable pupil size, and a real-time view of the subject's pupil.

1. Test Channel
A 543-nm He–Ne laser produces light for the test channel. The coherence of the laser light is broken by a rotating diffuser. The light is then collimated by a lens and used to illuminate a spherical mirror of short focal length: a 12-mm steel ball (R_3). The reflection from the steel ball produces a divergent, high-numerical-aperture beam (N.A., ~1), which the subsequent optics image as a point source. Light from the point source focuses from a gimbaled mirror (Fourward Technologies) that is controlled by an analog joystick. Adjusting the angle of the joystick allows the subject to change the angle of the mirror rapidly in two dimensions. Tilting the mirror changes the angle at which the test beam enters the eye and therefore changes the retinal location of the test spot. We select the pupil entry position of the test beam from a set of 1-mm holes that tile the pupil of the eye, location P_2 (Fig 1, inset) by rotating a metal wheel that is optically conjugate to the pupil of the eye. The wheel is constructed such that it can be rotated to one of 37 preset locations. At each location a single sampling aperture is located within the pupil of the system. Thus, by simply rotating the wheel, we can rapidly vary the pupil entry position of the test beam across the eye's pupil. Because the pupil selection wheel is located after the gimbaled mirror, the

combination of the two control systems allows us rapidly and independently to adjust both the entry position of the test beam into the eye and the angle at which the test beam enters the eye.

2. Pupil-Monitoring Channel
All measurements are referenced to the entry location of the test channel within the pupil of the eye. We align the center of the pupil of the eye to the optical axis of the system by using an infrared-sensitive CCD video camera. This camera is located behind a cold mirror (transmitting near infrared) in the test channel and provides a magnified view of the eye's pupil. The camera is set such that the depth of field is roughly 2 mm. An acetate overlay with a series of concentric circles is mounted upon the video monitor. The circles are centered on the optic axis of the instrument. We constructed the acetate sheet by imaging through the camera a calibrated set of circles located at the exit pupil and centered on the optic axis. Thus the center of the circles on the overlay indicates the actual position of the optic axis when the circles are viewed through the video camera and monitor. The experimenter aligns the subject's pupil to the concentric circles by manipulating a three-dimensional (X, Y, Z) translator upon which the subject's bite bar is mounted. A foam headrest provides added stability for the subject. During the experimental session the eye is continuously visible on the video monitor, with the alignment circles overlaying the image of the pupil.

3. Fixation Channel
The fixation target, typically a cross, is provided by a second optical channel. The fixation channel is illuminated by a tungsten–halogen bulb, relayed through a large (8-mm-diameter) fiber-optic illuminator. The end of the illuminator (Fig. 1, P_2') is conjugate to the pupil. Light from the illuminator is collimated and then passes through a filter holder–slide holder located in a retinal conjugate plane (Fig. 1, R_2'). We place an alignment–accommodation–fixation target (typically a cross), as well as neutral-density and colored filters, in the slide holder. We use a green filter (Kodak, Wratten 58) to match approximately the wavelength of the fixation channel to the test channel. Finally, the end of the fiber-optic illuminator is imaged on an adjustable iris diaphragm located in a pupil conjugate plane (Fig. 1, P_1'). The iris diaphragm allows us to adjust the diameter of the pupil from 0.5 to 7.0 mm. For most measurements this diaphragm is set to 1-mm diameter, matching the size of the sampling pupil. However, for conditions in which we are measuring the wave-front properties of the eye when it is accommodating, we increase the reference pupil diameter to 6 mm, providing a better stimulus for the accommodation system. The fixation channel is combined with the test- and pupil-monitoring channel at a beam splitter (Fig. 1, BS).

4. Refraction Control
All three channels pass through a common refraction control system. This consists of a set of mirrors mounted on a movable stage. By translating the mirrors we can precisely vary the distance between the Maxwellian lens and the image of the point source (Fig. 1, R_1). This refraction
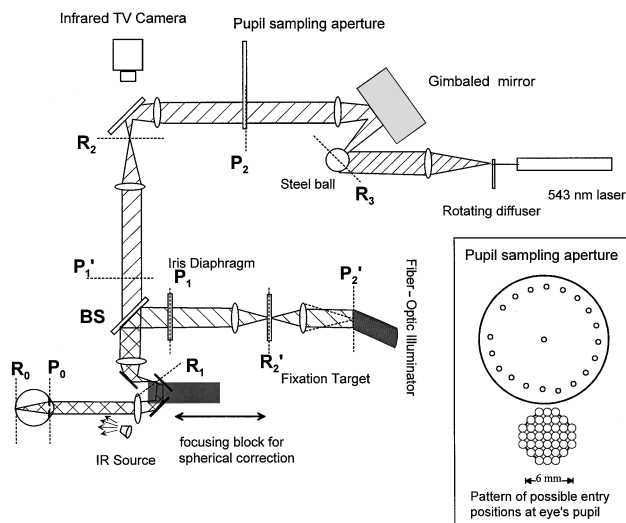

Fig. 1. Schematic diagram of the spatially resolved refractometer. It is a three-channel Maxwellian view system (see text), which has separate channels for the test, the fixation stimulus, and pupil monitoring. A Badal optometer (focusing block) allows the experimenter to change the refractive state of the test and reference channels together, without changing the location of the pupil (P_0) conjugate planes (P_1, P_1', P_2, P_2'). Retinal (R_0) conjugate planes are located at positions R_1, R_2, R_2', and R_3. (Other abbreviations are defined in the text.) All lenses have a focal length of 150 mm and a diameter of 35 mm.

control thus permits correction for a spherical refractive error of as much as -6 diopters (D). We allow subjects to adjust best focus with the fixation channel pupil set to 6 mm. When we are measuring accommodation for ametropic subjects we insert the appropriate trial lenses into the instrument at locations P_1 and P_1' to match the dioptric equivalent of the subject's best focus and then use the focusing block to precisely vary the accommodative stimulus.

B. Calibration

The spatially resolved refractometer was calibrated in three steps. First, we determined the actual sample positions of the sample apertures at the plane of the eye's pupil by placing a calibrated CCD chip at the exit pupil of the system (plane P_0 in Fig. 1). The pixel-to-pixel spacing of the CCD was 24 μm. A 1:1 image of the sampling aperture in the selection wheel was then obtained for each of the 37 positions. We used computer processing to find the center of the image of the exit pupil. We confirmed that the sampling apertures formed an almost perfect grid, with centers spaced at 1 mm.

Second, we measured the relation between the deviation angle of the gimbaled mirror and the joystick voltage by increasing the intensity of the test beam and projecting it onto a wall behind the apparatus. By measuring the distance to the wall, and the position on the wall for a series of joystick voltages, we could compute the angular deviation of the beam. This control system was linear, with a correlation coefficient between the analog-to-digital value and the angle greater than 0.999.

Finally, we placed a CCD television camera with a diffraction-limited lens in place of the subject's eye. Then, while watching a video monitor, we confirmed that the image of the point source did not vary as the sample aperture changed position.

C. Subjects

We made measurements on six subjects; two females, S1 and S2 (both age 26), and four males, S3–S6 (ages 28, 34, 37, and 47). The refractive errors of the subjects ranged from emmetropic to -5.56 D. Other than exhibiting refractive errors, all subjects were ocularly normal. Three of the subjects (S1, S3, and S6) participated in repeat measurements spaced over 1 month.

D. Test Procedure

At the start of each experimental session we aligned the subject to the apparatus by positioning a bite bar and head rest, using an X–Y–Z positioning stage. Once the subject was aligned, an image of the pupil was collected from the infrared monitor by a video frame grabber in the control computer. The image was stored for later analysis of the actual location of the pupil within the session. In addition, the experimenter monitored the subject's pupil on the video screen and adjusted the head position with the X–Y–Z positioning stage if needed. Each experimental run consisted of a complete set of 39 measurements of the angle required for aligning the test spot to the fixation target (typically, the center of a cross that extended across the entire background field). The first and last measurements in each run were collected with the

sampling pupil centered in the exit pupil of the apparatus. The other 37 measurements, including one additional measurement for central pupil entry, were presented in a pseudorandom order. The subject's task was to align the test stimulus to the center of the fixation cross by using the method of adjustment. The subject indicated when the test spot was located at the center of the fixation cross without moving from the bite bar. In general, all subjects could complete the 39 measurements for each run within 4 min. The three repeat measurements obtained with central pupil entry were used as a measure of the variability within a run and informally for detecting any equipment problems during a run, although for the current data set no such problems were encountered. After each set of 39 measurements the experimenter saved the data to disk, changed stimulus conditions, if needed, and another set of measurements was collected. Since we were able to perform this task at a low retinal illuminance (<100 trolands), no dilation of the pupil was necessary. Thus, except where noted, all measurements are for the natural pupil and lens and with free accommodation.

E. Data Analysis

The data recorded by the computer are measures of the slope of the wave front at each point in the pupil. The more common measure of optical aberrations is the deviation of the height of the wave front from a plane wave as a function of pupil location. We used a least-squares procedure[22,23] to fit the slope measurements to a set of Zernike polynomials[24,25] to approximate the wave-front height.[26] The advantages of the Zernike polynomials for this purpose have been discussed elsewhere.[24,25,27–30] Briefly, they allow an efficient, mathematically complete description of the variation of the wave front across the pupil. By decomposing the wave front into a series of coefficients that describe the contributions of the various Zernike terms, we can decompose the wave front in a way that is similar to the Fourier decomposition of a time- or space-varying stimulus. Thus the Zernike coefficients express the amplitude of variation in height contributed by each term of the Zernike series. Classic optical properties can be computed from some of the Zernike coefficients; for example, cylinder is a combination of the third and the fifth coefficients. However, other Zernike terms have no equivalent Seidel terms.[30] The 37 sampling points in our measurement configuration allowed us to fit up to the seventh order of the Zernike expansion (35 terms). We used the coefficients of the first 35 Zernike terms to estimate the continuous wave front of the eye's pupil.

F. Simulations

There are several potential artifacts that one may encounter in using a least-squares fit Zernike expansion on a finite data grid. First, for a small data set, the Zernike polynomials are not orthogonal; this means that, if there is power at orders higher than are fitted, the actual lower-order power may be misestimated.[31] Second, even with dense sampling, the slopes of the Zernike polynomials are not orthogonal.[32] Finally, the typical analysis implicitly assumes that the slope of the wave front is being esti-

mated at a single location in the pupil. In actuality a finite-sized sample pupil is used, and the measured deviation of the test spot is an estimate of the wave-front slope across this finite pupil. To test the robustness of our technique to these two factors we performed extensive numerical simulations of the measurement technique. A set of MATLAB (Mathworks, Natick, Mass.) programs was written that could produce wave-front distributions with power up to the ninth order (54 coefficients). The spatial distribution of the slope of the simulated wave front was then computed with respect to the horizontal and vertical axes. These slope distributions were averaged for each of our sampling aperture positions.[31] The resultant average slope data were then used as input to the standard analysis routines, and the resultant coefficient expansion was compared with the originally specified coefficients.

3. RESULTS

A. Simulations
The simulation revealed that the presence of higher-order aberrations in large amounts could cause systematic errors in the estimation of the power present in the lower orders. Figure 2 shows one example of the results from the simulations. We generated these data by first setting coefficients for the 3rd through the 35th Zernike terms such that they were basically decreasing with increasing order but with some randomness added. We next added to them the coefficients for the 36th through the 54th terms of the Zernike expansion. The values of these coefficients were set such that they decreased the Strehl ratio of the wave front to 0.54 when coefficients 1–35 were all set to zero. This choice of high-order coefficients represents more high-order aberrations than are estimated to be present in human eyes,[13] so our estimate of the effect of high-order aberrations should be conservative. Finally we generated the composite wave front, numerically determined from the coefficients, calculated the slopes, and used the standard fitting routine to extract coefficients 3–35. As can be seen from Fig. 2, the simulated measurements (filled circles and dashed curve) deviate somewhat from the actual coefficients (solid curve).
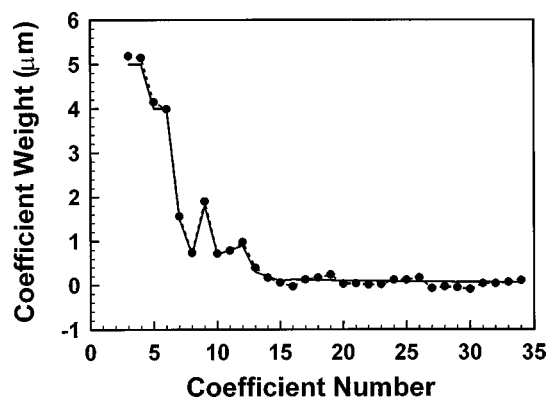

Fig. 2. Example of the results of the numerical simulations of the effect of high-order aberrations on the measured Zernike coefficients. Solid curve, values entered into the simulation program for Zernike coefficients 3–35. Filled circles, predicted measurements. We added sufficient high-order aberrations (coefficients from 36 to 54) to decrease the Strehl ratio to 0.54.

However, in all cases the deviations are small (average deviation, 0.081 ± 0.058). This low sensitivity to the presence of higher-order aberrations derived in part from our use of a 1-mm sampling aperture. Reducing the simulated size of the sampling aperture from 1 to 0.05 mm in diameter, while keeping our sampling grid constant, increased the effect of the higher-order aberrations by 13%.

We also found that the use of the larger sampling aperture increased the effect of aliasing of the Zernike terms between the 20th and the 35th into the lower-order terms. This effect depended on the exact sampling geometry used. We found that, while our sampling geometry was adequate to measure wave-front aberrations in normal eyes, it could be susceptible to aliasing artifacts in eyes with large amounts of high-order aberrations.

Finally, our simulations revealed that the spatial averaging across our sample pupil caused a small but systematic decrease in our sensitivity to lower-order aberrations as well. That is, our measurements tended to underestimate the amount of actual wave-front height variation that arose from the fifth- through seventh-order terms. This effect represents an underestimation of only a few percent and for the data reported here (where the high-order aberrations were relatively small) should not be significant.

B. Accuracy
We tested the accuracy of the spatially resolved refractometer by mounting a television camera with a diffraction-limited lens in place of the eye. The experimenter aligned the images of the test spot to the image of the reference cross on a video monitor. Other than in the use of the camera, this configuration simulated all aspects of the experimental session. With the camera lens alone there were no measurable aberrations. We next introduced blur into the system either by introducing trial lenses or by moving the refraction block, and repeated the measurements. Figure 3a shows the derived Zernike coefficients for spherical defocus of 1.3, 0, and -1 D. The coefficient weights are plotted in terms of the amplitude of the wave-front deviation produced by each term. That is, an amplitude of 1 in the defocus term means a peak-to-trough change in height of approximately 2 μm across the pupil ($+1$ μm).[33] Note that only the fourth coefficient (defocus) changed, confirming that defocus alone, for a high-quality lens, does not increase the measured aberrations. In addition, we confirmed that all coefficients were near zero if the system was focused at infinity (mean, 0.006 ± 0.051). Overall we were able to measure accurately the defocus produced by a trial lens over a roughly 5-D range. This limitation in the instrument arises from the size of the angle (0.024 rad) that we can impose on the gimbaled mirror by using the current optics. However, because the refraction control system can be varied over 6 D, the total range of the instrument is much larger. The 5-D range is adequate for the aberrations present in most normal eyes but may not be sufficient for an eye with very irregular optics, as would be found with corneal scars, or for multizone corneas.
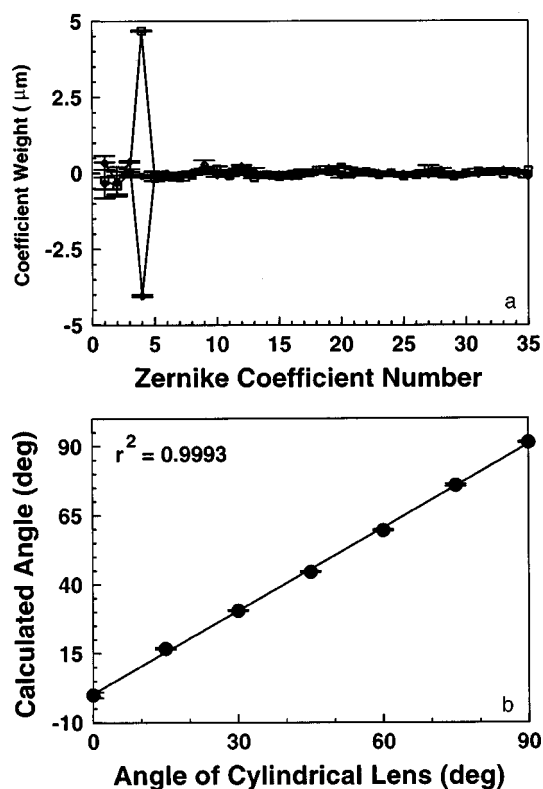
Fig. 3. a, Data collected from the spatially resolved refractometer with a CCD camera in place of the eye. Data are shown for three different levels of defocus: -1, 0, and 1.3 D. We have not plotted either piston (the zero-order Zernike term) or tilt (the first-order Zernike terms). The horizontal line near each data point represents plus or minus one standard deviation of the measurements. b, Measured angle of a 2-D cylindrical lens as a function of its actual angle. Horizontal lines, plus or minus one standard deviation of the measurements.

Figure 3b plots the angle of the astigmatic axis derived from the third and fifth coefficients of the Zernike expansion as the actual angle of a cylindrical lens was rotated.

C. Measurements on Subjects

1. *Reliability of Measurements*

We assessed the repeatability of data collected from the subjects by examining the repeatability of the data for the central pupil entry within a single run, by examining the variability of repeat runs within a single session, and by examining the repeatability of measurements across days. The standard deviation within a single run was computed as the grand average, across both sessions and subjects, of the three repeat matches of the test to the standard when the sampling aperture was centered on the optical axis of the instrument. On average, the standard deviation of these matches was 0.00027 rad, while the total range of the equipment was 0.024 rad. For comparison, if 0.00027 rad were to arise from purely defocus measured at the edge of a 6-mm diameter pupil, it would be equivalent to a 0.09-D blur, which is an almost noticeable blur. Figure 4a shows the average Zernike coefficients for subject S1 computed from five separate runs within a single session. The error bars indicate the entire range of the coefficients obtained across the five runs, not the standard deviation. The runs were highly re-

peatable, and the standard deviation for the five runs averaged 0.19 μm per coefficient. Similar results were obtained for subjects S6 and S3. Typically we used the coefficient representation of the wave-front measurements to calculate the wave-height variation across the pupil. Figure 4b shows the related standard deviation of the wave-height estimates. To make these calculations we reconstructed the wave height for the five runs of the top panel and then calculated the standard deviation of the wave heights for each point in the pupil. We then calculated the radial averages of the standard deviations
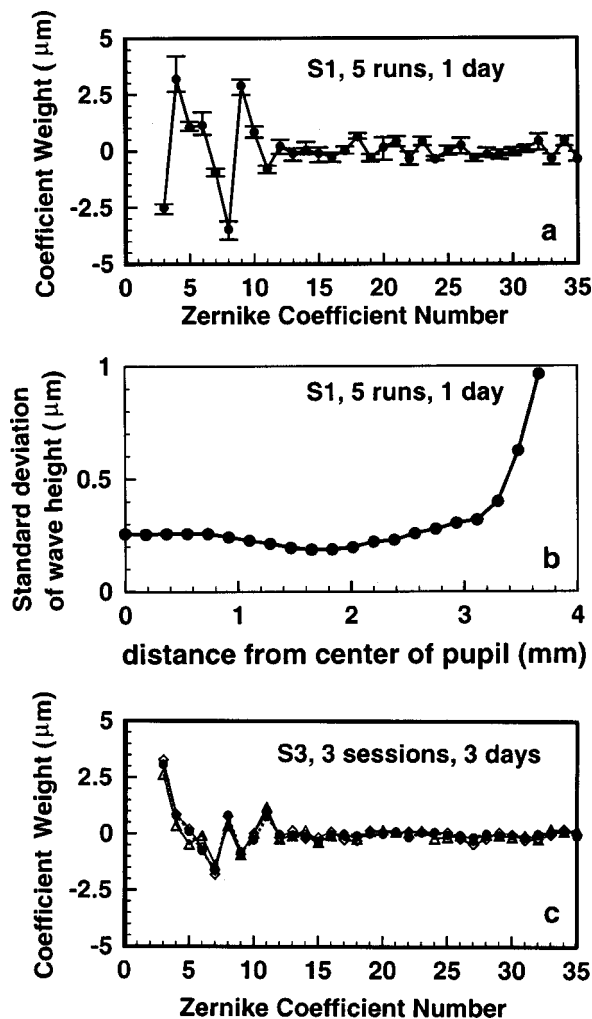

Fig. 4. a, Zernike coefficients estimated from five successive runs in a single session from subject S1. The filled circles and the solid curve plot the mean of the five runs. The error bars indicate the range of the coefficient estimates for the five runs. This subject's aberrations were dominated by coma (Zernike terms 7 and 8) as well as by other terms that do not have classical optical equivalents. The average standard deviation for the 3rd through the 10th coefficients was 0.48 μm. b, Standard deviation of the wave-height estimates obtained from five consecutive runs collected on a single day (observer S1). The standard deviation of the wave height was first computed for each point in the pupil. These data were then radially averaged, giving the standard deviation as a distance from the center of the pupil. At the edges of the pupil the standard deviation estimates increased sharply, probably because only the edges of six of the sample pupils were located at this distance from the center of the pupil. c, Comparison of Zernike coefficient estimates gathered from subject S3 on three separate days spanning a month. Each curve is the average estimate for that day.
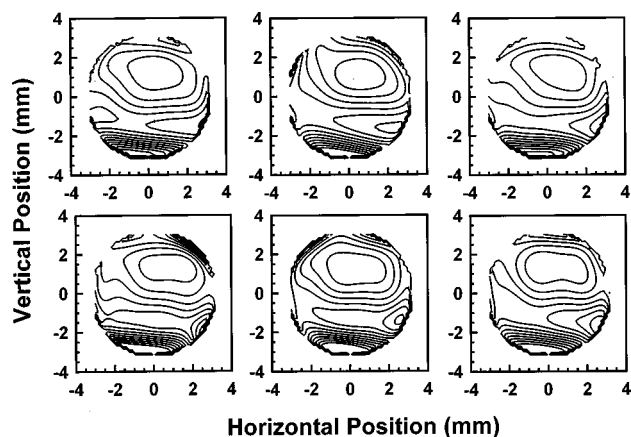
Fig. 5. Wave-front height contours for subject S1. Contours are calculated for a 7.32-mm pupil and are spaced at 1-μm intervals. Defocus was excluded from the calculation of the wave front. Top row, plots from three sequential runs collected in a single day. Bottom row, three sequential runs from a different day.

as a function of the distance from the pupil center. These values varied from 0.2 to 0.3 μm, except at the edges of the pupil. Figure 4c shows estimates of the Zernike coefficient weights gathered on three separate days for subject S3. The data for each day are the average obtained across all appropriate runs collected on that day ($n = 2, 3, 5$). The data presented are for the best focus condition, as subjectively determined. The data were collected over 1 month. The good reliability of our estimates of the Zernike coefficients both for data collected in a single day and for data collected across several days is also represented in the repeatability of our estimates of the total wave-front variation.

Figure 5 shows wave-front contour plots for subject S1. The top row plots three wave-front estimates from three single sessions on the same day. The bottom row plots three additional measurements obtained on a different day. The general features of the wave front, which in this subject represent predominantly coma, reproduced extremely well, even producing the same noncentral region of the shallowest wave-front curvature. Note that, in all cases, the day-to-day and run-to-run variability in the shape of the wave fronts was similar.

As in previous studies, we found that the spatial distribution of wave-front variations, though consistent within a subject, varied markedly across subjects. Figure 6 shows the average wave-front contours for the six subjects participating in this study. For these plots the defocus Zernike coefficient was set to zero, and contours were drawn at 1 μm intervals. The individual differences shown were all reliable across sessions for each of the subjects.

2. *Measurement of Changes in Wave Front*

Figure 7 compares wave-front contours for subjects S1 (top row) and S3 (bottom row) under different conditions. For all wave fronts we subtracted the effect of the defocus term from the wave front. For the wave-front data displayed in the leftmost panels each subject was fixating a target at his or her resting state of accommodation. For the data in the central panels, each subject's test eye was

dilated with 0.5% tropicamide. These data were collected on the same day, in sessions immediately following the measurements shown in the left most panels, with no intervening changes to the equipment or to the position of the bite bar. There was a clear, but relatively small, change in the wave front with mydriasis, which for both subjects represented a total change of roughly 2 μm across the pupil of the eye. For a 6-mm-diameter pupil this change in wave front corresponded to a decrease in the Strehl ratio from 0.17 to 0.10 for subject S3 and from 0.079 to 0.078 for subject S1. We also analyzed the change in the individual Zernike coefficients. There were significant changes in some but not all coefficients. For both subjects there was a change in defocus, indicating that the subjects did not maintain the same plane of focus, even though the stimulus was identical. Other than in defocus, the largest change in the Zernike coeffi-
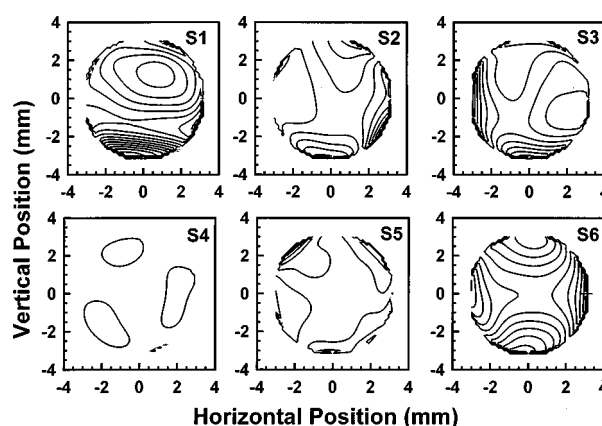

Fig. 6. Wave-front maps for all six subjects. Contours are plotted at 1-μm intervals and do not include defocus but do include all other Zernike terms up to 35. The variation among individuals in the optical quality of the eye is evident. Subject S4, for instance, has only approximately 1 μm of aberrations across his entire pupil.
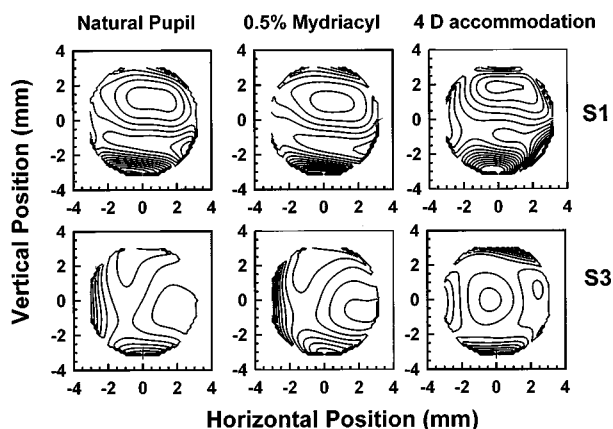

Fig. 7. Comparison of wave-front maps for subjects S1 and S3 under different experimental conditions. Leftmost column, data collected with free accommodation to a target at the subject's far point. Middle column, data collected from the same subjects but after administration of 0.5% tropicamide to dilate the pupil. These data were collected under identical conditions to those that produced the data in the leftmost column, including bite bar and target positions. Rightmost column, data collected when the refraction control is used to generate a 4-D accommodative stimulus.

cients was in astigmatism, but significant changes were present for higher-order coefficients as well, although which coefficients changed varied across subjects. If changes in focus were significant within a run, then we might expect a difference in the standard deviation of the settings when the pupil was pharmacologically dilated. However, there was not a significant change in the standard deviation of the settings between the mydriatic and natural pupil data. This result suggests that measurements with the natural pupil are as reliable as measurements with the artificially dilated pupil. In addition, the standard deviation of the defocus coefficient was not larger than the standard deviation of the other coefficients, again indicating that there was not a problem with the subjects' maintaining their accommodation during the run.

For the data in the rightmost panels of Fig. 7 the target was moved by use of the refraction control system to generate a 4-D accommodation stimulus. Subjects' eyes were not dilated. There is a significant increase in the amount of aberrations measured across the pupil with accommodation.[34] These changes occurred for higher- as well as for lower-order aberrations. For instance, for observer S3 coefficient 10 increased by 1 μm, which should be a readily noticeable increase in aberrations because it produces a deflection of the test beam much larger than the standard deviation of the measurements.

4. DISCUSSION

A. Fitting Procedure

While the Zernike polynomials are mutually orthogonal on an infinite set of points within an aperture, they are not orthogonal for a finite sampling of the pupil, and their derivatives are not orthogonal even with dense sampling.[13] In principle this phenomenon leads to interactions between orders; if there are higher orders of aberrations present than are being fitted, then the estimates of the power present in the lower orders may be erroneous. For instance, if we were to use a small set of coefficients (say, the first 21) but there is finite power in the higher-order terms that is not extracted, systematic errors in the computations of the low-order coefficients can result. We minimized this error both by extracting the complete set of allowed coefficients (35 coefficients for the 37 sampling locations) and by using a relatively large sampling aperture (1 mm), which practically tiled the measured extent of the pupil. The simulations supported the assumption that the use of a large sample pupil decreases our sensitivity to higher orders of wave-front variations by averaging the wave front over the spatial extent of the sample pupil. In sampling terms, the use of a large sample pupil is a low-pass filtering operation; the finite size of this aperture smooths the resultant data on a 1-mm spatial scale. However, the simulations also revealed that other sampling errors were introduced by the sampling aperture size. These errors arose from two related factors, the use of the value of the derivatives at the center of the sampling apertures to perform the fitting and the nonideal sampling that a rectangular sampling array provides for radial basis functions. Despite these problems, the simulations confirmed that the overall ef-

fect of this nonideal behavior is relatively small for our conditions. However, it is important to note that these effects may not be small if either a different sampling array or eyes with high amounts of higher-order aberrations are tested. In general, it is desirable to perform the simulations for any new experiment or testing situation.

B. Sensitivity of the Psychophysical Technique

From measurements of both spherical and astigmatic trial lenses we determined that the spatially resolved refractometer accurately measures optical defocus and astigmatism. Targets that generate known amounts of high-order aberrations were not available to us. However, none of the measurements on the spherical and cylindrical lenses generated significant amounts of high-order aberrations, indicating that our measurements of these higher-order aberrations in the eyes of our subjects were real. Our simulations suggest that our measurements may represent a slight underestimate of the total aberrations of the eye but should not be an overestimate. In addition, we found that the high-order aberrations measured in human eyes were reproducible and varied in systematic ways from one subject to the next.

We also found that the technique was reproducible. Repeat measurements within a day and across days differed mainly in the defocus coefficient; other coefficients could be estimated to better than 0.1 μm (the standard error of 5 runs, averaged across all 35 coefficients). The variation in defocus was to be expected; because the subjects' accommodation was not interfered with pharmacologically, they were allowed to accommodate freely. When defocus was mathematically subtracted from the wave-front maps, the results were highly reproducible in a single subject both within and across days. In fact, each individual seemed to have a characteristic aberration pattern that was maintained over time and also was changed characteristically by accommodation.

It was previously reported that there is a change in tonic accommodation with the application of mydriatics,[35] a result that we also measured. However, we also found a change in the aberrations of the eye with the application of mydriatics. The measured changes were not large but were significant.

5. CONCLUSIONS

Psychophysical measurements of the wave-front aberrations of the eye can be made in a rapid, reproducible manner. This opens the possibility of studying changes in the aberration structure of the eye in conditions when mydriatics may interfere with the normal optics, such as when one is accommodating. The results obtained with free accommodation are not significantly more variable than those obtained with artificially dilated pupils, although we did not use more-powerful drugs to paralyze accommodation. In addition, the technique used is quite fast: Even the subjects without psychophysical experience were able to complete a single session within approximately 4 min. This result makes the technique a practical candidate for measuring wave-front aberrations in subjects for whom the objective techniques may not work well, such as patients with mild ocular opacities. The

alignment task used in this test is resistant to mild optical degradation. Subjects can align a large blurred image of the point source to the center of the reference target quite well, a result that was borne out in our calibration experiments with the video monitor, for which the experimenters were able to do this with high accuracy on the video monitor. For use out of the fovea this technique may have to be modified, because vernier acuity is degraded away from the fovea; however, an objective version of this technique has been described.[11,21] Within the range of conditions for which it works, the technique has a number of important strengths and can be used to study the change in the wave-front aberrations of the eye under a variety of physiological conditions.

ACKNOWLEDGMENTS

REFERENCES AND NOTES

1. P. Artal, S. Marcos, I. Iglesias, and D. G. Green, "Optical modulation transfer function and contrast sensitivity with decentered small pupils in the human eye," Vision Res. **36**, 3575–3586 (1996).
2. P. Artal and R. Navarro, "Monochromatic modulation transfer function of the human eye for different pupil diameters: an analytical expression," J. Opt. Soc. Am. A **11**, 246–249 (1994).
3. F. W. Campbell and R. W. Gubisch, "Optical quality of the human eye," J. Physiol. (London) **186**, 558–578 (1966).
4. J. A. M. Jennings and W. Charman, "An analytical approximation of the transfer function of the eye," Br. J. Physiol. Opt. **29**, 64–72 (1974).
5. R. Navarro and M. A. Losada, "Phase transfer and point-spread function of the human eye determined by a new asymmetric double-pass method," J. Opt. Soc. Am. A **12**, 2385–2392 (1995).
6. C. Cook, J. Koretz, A. Pfahnl, J. Hyun, and P. Kaufman, "Aging of the human crystalline lens and anterior segment," Vision Res. **34**, 1945–2954 (1994).
7. A. Glaser and M. C. W. Campbell, "Presbyopia and the optical changes in the human crystalline lens with age," Vision Res. **38**, 209–229 (1998).
8. J. Koretz, C. Cook, and J. Kuszaks, "The zones of discontinuity in the human lens: development and distribution with age," Vision Res. **34**, 2955–2962 (1994).
9. P. Artal, J. Santamaria, and J. Bescos, "Retrieval of wave aberration of human eyes from actual point-spread-function data," J. Opt. Soc. Am. A **5**, 1201–1206 (1988).
10. G. Walsh, W. N. Charman, and H. C. Howland, "Objective technique for the determination of the monochromatic aberrations of the human eye," J. Opt. Soc. Am. A **1**, 987–992 (1984).
11. R. Navarro and M. A. Losada, "Aberrations and relative efficiency of light pencils in the living human eye," Optom. Vision Sci. **74**, 540–547 (1997).
12. J. Liang, B. Grimm, S. Goetz, and J. F. Bille, "Objective measurements of wave aberrations of the human eye with the use of a Hartmann–Shack wave-front sensor," J. Opt. Soc. Am. A **11**, 1949–1957 (1994).
13. J. Liang and D. R. Williams, "Aberrations and retinal image quality of the normal human eye," J. Opt. Soc. Am. A **14**, 2873–2883 (1997).
14. H. C. Howland and B. Howland, "A subjective method for the measurement of monochromatic aberrations of the eye," J. Opt. Soc. Am. **67**, 1508–1518 (1977).
15. M. C. W. Campbell, E. M. Harrison, and P. Simonet, "Psychophysical measurement of the blur of the retina due to optical aberrations of the eye," Vision Res. **30**, 1587–1602 (1990).
16. R. Woods, L. A. Bradley, and D. A. Atchison, "Monocular diplopia caused by ocular aberrations and hyperopic defocus," Vision Res. **36**, 3597–3606 (1996).
17. W. N. Charman, "Wavefront aberration of the eye: a review," Optom. Vision Sci. **68**, 574–583 (1991).
18. R. H. Webb, C. M. Penney, and K. P. Thompson, "Measurement of ocular wavefront distortion with a spatially resolved refractometer," Appl. Opt. **31**, 3678–3686 (1992).
19. A. Ivanoff, "Sur une methode de mésure des aberrations chromatique et spheriques de l'oeil en lumière dirigée," C. R. Hebd. Seances Acad. Sci. **231**, 562–528 (1946).
20. A. Ivanoff, "About the spherical aberration of the eye," J. Opt. Soc. Am. **46**, 901–903 (1953).
21. C. M. Penney, R. H. Webb, J. T. Tieman, and K. P. Thompson, "Spatially resolved objective refractometer," U.S. patent 5,258,791 (November 2, 1993).
22. R. Cubalachini, "Modal wavefront estimation from wavefront slope measurements," J. Opt. Soc. Am. **69**, 972–977 (1979).
23. W. Southwell, "Wavefront estimation from phase derivative measurements," J. Opt. Soc. Am. **70**, 998–1006 (1980).
24. V. N. Mahajan, "Zernike circle polynomials and optical aberrations of systems with circular pupils," Appl. Opt. **33**, 8121–8124 (1994).
25. D. Malacara, *Optical Shop Testing* (Wiley, New York, 1992).
26. We used the convention described by Malacara[25] for determining which coefficient represents each polynomial. In this system, defocus is represented by the fourth coefficient, first-order astigmatism by a combination of the third and the fifth, coma by the seventh and the eighth, and first-order spherical aberration by the twelfth.
27. M. Born and E. Wolf, *Principles of Optics* (Pergamon, Oxford, UK, 1983).
28. J. Schwiegerling, J. E. Grievenkamp, and J. M. Miller, "Representation of videokeratoscopic height data with Zernike polynomials," J. Opt. Soc. Am. A **12**, 2105–2113 (1995).
29. J. Y. Wang and D. E. Silva, "Wave-front interpretation with Zernike polynomials," Appl. Opt. **19**, 1510–1517 (1980).
30. R. H. Webb, "Zernike polynomial description of ophthalmic surfaces," Ophthalmic Visual Opt. **3**, 38–41 (1992).
31. J. Herrman, "Cross coupling and aliasing in modal wavefront estimation," J. Opt. Soc. Am. **71**, 989–992 (1981).
32. These measurements are traditionally adjusted with a Gram–Schmidt procedure (see Ref. 25). However, we have not found this necessary because we are not using a point sampling procedure (see results).
33. This is true for all terms that we used except the 12th term, which has a lower peak-to-peak amplitude.
34. D. A. Atchison, M. J. Collins, C. F. Wildsoet, J. Christensen, and M. D. Waterworth, "Measurement of monochromatic ocular aberrations of human eyes as a function of accommodation by the Howland aberroscope technique," Vision Res. **35**, 313–323 (1995).
35. B. Gilmartin and R. E. Hogan, "The relationship between tonic accommodation and ciliary muscle innervation," Invest. Ophthalmol. Visual Sci. **26**, 1024–1028 (1985).